Concatenated tandem constructs of BK channels reveal three distinct types of subunit stoichiometry in channel modulation by the auxiliary γ subunit and mutations in the channel pore region

Guanxing Chen[1], Qin Li[1], Jiusheng Yan[1,2]

[1]Department of Anesthesiology and Perioperative Medicine, The University of Texas MD Anderson Cancer Center, Houston, Texas, USA

[2]Neuroscience and Biochemistry and Cell Biology Graduate Programs, MD Anderson UT Health Graduate School of Biomedical Sciences, Houston, Texas, USA

Abstract

The large-conductance, Ca^{2+}-activated K^+ (BK) channels consist of the Ca^{2+}- and voltage-sensing and pore-forming α (BKα) subunits and regulatory auxiliary β or γ subunits. Concatenated tandem constructs have been proved to be necessary and powerful in understanding the subunit stoichiometry of K^+ channel gating and regulation by constraining the stoichiometry, organization, and mutation of individual subunits. However, because of its unique possession of an extra S0 transmembrane segment that puts the N- and C-termini on the opposite sides of the membrane, it is impossible to generate concatenated tandem subunit constructs of BK channels as those done with other K^+ channels. In order to investigate the molecular mechanisms of the atypical "all-or-none" modulatory function of the γ subunits and the subunit stoichiometry of BK channel gating, we have taken a novel strategy and generated functional concatenated tandem constructs containing 2 or 4 copies of the BKα subunits by splicing BKα into 2 protein constructs that can be co-expressed to form functional channels. We observed that the BK channels formed by concatenated tandem constructs are similar to intact channels in voltage and Ca^{2+} gating properties. Interestingly, the BKγ1 subunit and mutations located at the S6 transmembrane segment and selectivity filter displayed 3 distinct types of subunit stoichiometry in BK channel modulation. By fusion of the BKγ1 subunit to the N-terminus of the concatenated tandem BKα constructs, we observed that a single molecule of BKγ1 subunit per tetrameric BKα channel is sufficient to fully modulate the channels. The Y294K, F303A, and L312A mutations at each BKα subunit has an incremental effect on BK channel gating. The V288A mutation at the selectivity filter produce an "all-or-none" effect but requires mutations at all 4 BKα subunits to have modulatory effect on channel gating, i.e., mutations at 1, 2, or 3 subunits have nearly no effect. Interestingly, the F307A mutation exhibited an atypical "all-or-none" modulatory function similar to that of the γ1 subunit. The diversity in subunit stoichiometry of BK channel modulation indicates distinct mechanisms in affecting BK channel gating. Overall, we have developed novel concatenated tandem constructs for BK channels and revealed three distinct types of subunit stoichiometry in BK channel modulation by the auxiliary γ subunit and mutations at the pore-lining S6 transmembrane segment and selectivity filter.

Introduction

The big/large-conductance, calcium- and voltage-activated K^+ (BK) channel is a unique member of the potassium channel family, characterized by an exceptionally large single-channel conductance (200-300 pS) that is 10-20 times larger than that for most other K^+ channels and dual regulation by membrane voltage and intracellular free Ca^{2+} ($[Ca^{2+}]_i$)[1,2]. The BK channel is a homotetrameric channel consisting of 4 identical subunits of the pore-forming, Ca^{2+}- and voltage-sensing α (BKα) subunit (~130 kDa) and variable regulatory auxiliary subunits. 3D structures of BKα channels[3-8] are informative in molecular architectures and allosteric gating mechanisms. In the transmembrane (TM) domains, BK channels differ greatly from Kv channels by possession of an extra S0 helix, lack of domain swapping between the S1-S4 voltage sensor domain (VSD) and the S5-S6 pore gate domain (PGD), and tight packing of the VSD against the PGD via extensive interactions between S4 and S5[5-8]. BK channels have a large cytosolic C-terminus composed of two tandem RCK domains (RCK1, RCK2) for Ca^{2+} and Mg^{2+} sensing[5,6,9-14] assembled into a tetrameric gating ring that expands and moves close to membrane in response to Ca^{2+}-bindings.

BK channel function is regulated by various auxiliary β and γ subunits and by LINGO1 protein, which confer tissue-specific gating and pharmacological properties[15-18]. The 4 BK channel β (BKβ) subunits are double membrane-spanning membrane proteins and they exert different and complex effects on apparent calcium and voltage sensitivities, macroscopic current kinetics, and pharmacological sensitivities[16,19-27]. The 4 BK channel γ (BKγ) subunits are a group of leucine-rich repeat (LRR) containing membrane proteins consisting of BKγ1 (LRRC26), BKγ2 (LRRC52), BKγ2 (LRRC55), and BKγ4 (LRRC38) [26,27]. They possess distinct capabilities in facilitating BK channel activation by shifting the BK channel's voltage dependence of activation in the hyperpolarizing direction over an exceptionally large range of ~145 mV (γ1), 100 mV (γ2), 50 mV (γ3), and 20 mV (γ4), in terms of the half-maximal

activation voltage ($V_{1/2}$) in the absence of Ca^{2+} [26,27]. BKγ1 likely modulated BK channels by mainly affecting the allosteric coupling between VSD activation and the channel pore opening[26,28].

All BKγ subunits contain an N-terminal signal peptide, an extracellular leucine-rich repeat (LRR) domain, a single transmembrane (TM) segment, and a short intracellular C-terminus[26,27,29]. The modulatory effects of different γ subunits on BK channel voltage dependence are mainly determined by their single TM segments and C-terminal positively charged residue clusters [30,31]. The single TM segment accounts for about 100 mV in $V_{1/2}$-shifting capability of the γ1 and γ2 subunits, while the intracellular C-tails, particularly the juxta-membrane positively charged residue regions, contribute about 40-50 mV in $V_{1/2}$-shifting capability to the γ1 and γ3 subunits [31]. The LRR domains regulate the expression, cell surface trafficking, and "all-or-none" modulatory functions of the BKγ subunits [29,32].

A fundamental question in understanding how an auxiliary protein regulates an ion channel is the subunit stoichiometry. In the classic model of a tetrameric ion channel complex, most auxiliary subunits bind to the channel with 4-fold symmetry to mirror the pore-forming α subunit's 4-fold structural symmetry so that the channel-regulatory effect is expected to be incremental upon variation in the relative molecular ratio of the auxiliary subunit to core subunit. Many K^+ channel auxiliary subunits such as the BKβ subunits on BK channels [33], KCNE on KCNQ channels[34,35], and KChiP on Kv4 channels[36], indeed incrementally regulate the voltage dependence of channel activation in a titration-dependent mode. However, BK channel modulation by BKγ1 exhibited an atypical binary "all-or-none" phenotype in that the voltage-dependence of BK channel gating was either fully shifted to the negative voltage direction or unchanged when expression of the BKγ1 subunit was limited[37]. Concatenated tandem subunit constructs with 2 or 4 channel subunits fused together in a C-to-N-terminus manner have been employed extensively to investigate the stoichiometry, interaction, and cooperativity of core and auxiliary subunits, and mechanisms of voltage- and ligand-gated activation in various K^+ channels[34,38-43]. However, owing to

an extra S0 segment that puts N- and C-termini on opposite sides of the membrane, it is impossible to make directly concatenated BK channel subunit constructs as with other K^+ channels. To permit investigation of intersubunit interactions and to restrict mutations to individual subunits, in this study we have developed concatenated tandem constructs of BKα subunits by splitting the BKα subunit into different constructs and revealed three distinct types of subunit stoichiometry in BK channel modulation by auxiliary γ subunits and mutations at selectivity filter and deep-pore locations. This study provides new insights into the modulation of BK channels.

Materials and methods

Expression of BK channels in HEK293 cells

HEK293 cells were cultured in Dulbecco's modified Eagle's medium with 10% fetal bovine serum in a 5% CO_2 incubator. HEK-293 cells (ATCC) were transfected with plasmids using PEI 'MAX' (Polysciences Inc.) and subjected to electrophysiological assays 16-72 h after transfection. Recombinant cDNA constructs of human BK channel was used for their heterologous expression in HEK293 cells as previously described [29,31,44,45]. For the tetramer construction, monomeric constructs of BKα (GenBank accession number AAB65837) that was lack of S0 (residues 1-93) and RCK2 domains (residues 651-1236) were subcloned into pcDNA6 with V5 and His tags. Concatenated BKα dimer constructs were generated in pcDNA6 with the following design: BamHI-BKα (M1)-XhoI-BKα (M2)-V5-AgeI. Concatenated BKα tetramer constructs were generated in pcDNA6 with the following design: BamHI-BKα (M1)-XhoI-BKα (M2)-NotI-BKα (M3)-BsiWI-BKα (M4)-V5-AgeI. Concatenated BKγ-α construct was generated in pcDNA6 with the following design: HindIII-BKγ1- BamHI-BKα (M1)-XhoI-BKα (M2)-NotI-BKα (M3)-BsiWI-BKα (M4)-V5-AgeI. A recombinant cDNA plasmid encoding the human was used for expression of the BKα subunit alone. Mutant constructs were made with the QuickChange site-directed mutagenesis kit (Stratagene).

Electrophysiology

To record the BK channel currents, we performed patch-clamp recording of excised inside-out plasma membrane patches of HEK-293 cells for most concatenated BKα wild type and mutation constructs with symmetric intracellular and extracellular (pipette) solutions containing 136 mM $KMeSO_3$, 4 mM KCl, and 20 mM HEPES, pH 7.20. The extracellular solution was supplemented with 2 mM $MgCl_2$, and the intracellular solution was supplemented with 5 mM HEDTA without Ca^{2+} to create a virtually Ca^{2+} free solution. Whole-cell patch-clamp recording was performed for some mutation constructs with tinny currents. Single channel currents were measured at holding voltages from −120 mV to +120 mV. Recording electrodes, amplifier, sampling rate, data analysis et al. were as previously described [45]. Steady-state activation was expressed as the normalized conductance (G/Gmax) calculated from the relative amplitude of the tail currents (deactivation at -120 mV). The voltage of half-maximal activation ($V_{1/2}$) and the equivalent gating charge (z) were obtained by fitting the relations of G/Gmax versus voltage with the single Boltzmann function $G/Gmax= 1/(1+e^{-zF(V-V_{1/2})/RT})$. Experimental values are reported as means ± SEM.

Western Blot

As previously described [29], the cell lysate was incubated (4 °C for 2 h) with anti-V5 agarose affinity gel antibody produced in mouse (Cat# A7345 from Millipore Sigma). After three repetitive washes (10 min each time) with TBS buffer supplemented with 2% DDM, the captured proteins were eluted with 4% SDS. Mouse monoclonal anti-V5 antibody (Cat# R96125 from Invitrogen) at 1:10,000 dilution was used for immunoblotting. Protease inhibitor cocktail (Roche) was used throughout the procedure.

Results

A novel strategy and generated functional concatenated tandem constructs of the BKα subunits.

In this study, a novel strategy was employed to generate concatenated tandem subunit constructs of BK channels. The goal was to place the N- and C-termini of BKα on the same sides of the membrane. Due to the large size of the RCK domains, a three-protein construct approach was utilized. This involved splicing BKα into three protein constructs: the S0 transmembrane domain (residues 1-97), the RCK2 domain (residues 652-1236), and the rest (residues 94-651). These three constructs were co-expressed to form

functional channels, as depicted in **Figure 1C**. This strategy allowed for the successful generation of functional BKα subunits in the form of concatenated tandem constructs.

To validate our strategy, we co-expressed the S0 transmembrane domain, RCK2 domain and the left domains of BKα in HEK cells. We observed that the $V_{1/2}$ of co-expression of three pieces of BKα channel was 177.81 ± 1.51 mV in the absence of Ca^{2+}, which closely resembled that of the non-spliced monomeric BKα constructs (V1/2 = 172 ± 3 mV). Furthermore, in the presence of 10 μM Ca2+, both the wild-type (WT) and co-expressed BKα channels exhibited an increase in V1/2 by 155 mV and 147 mV, respectively (**Fig. 1A and 1C**). These results clearly demonstrated that co-expression of the three pieces of BKα domains will form a functional BK channel. To further investigate the concatenated tandem subunit constructs of BK channels, dimers and tetramers of BKα were constructed by fusing the N-terminal of one subunit to the C-terminal of the preceding subunit (**Figure 1A, 1D and 1E**). Western blot analysis confirmed the presence of the concatenated BK channel construct, as indicated by the predominant protein recognized by the V5 antibody (**Figure 1B**). By analyzing the voltage dependence of the channel activation, we observed that both the dimers and tetramer constructions induced similar shift in $V_{1/2}$ in the absent and present of 10 μM Ca^{2+}. In the presence of 10 μM Ca^{2+}, the BK dimers (Dimer-M1M2 and Dimer-M3M4) and tetramer channels exhibited V1/2 shifts of 156 mV, 158 mV, and 144 mV, respectively, compared to the absence of Ca^{2+} (**Fig. 1D-E, Table 1**). Indeed, the results obtained from our experiments unequivocally demonstrated that the tandem constructs of BKα, generated using our novel strategy, exhibited similar functional properties to the monomeric BKα constructs that were previously employed. This suggests that our novel approach of splicing BKα into three protein constructs successfully resulted in the formation of functional BK channels, allowing us to investigate the subunit stoichiometry and modulation of BK channels in a concatenated tandem format.

The deep pore L312A mutation on each BKα subunit has an incremental effect on BK channel voltage gating.

Previously, L312A mutant was identified to led to low-voltage–activated BK channels (L312A), and mutant leucine (L) to alanine (A) at position 312 would induce a 132 mV shift in the $V_{1/2}$ (31 ± 2.6 mV) toward the hyperpolarization direction as compared with wild type [46,47]. The L312 site is in the S6 transmembrane domain that located at the deep-pore position of BKα channel (**Figure 2A and 2B**). Similar to the previous reports [46,47], the voltage dependence of the BKα L312A mutant channels ($V_{1/2}$ = 61.9 ± 3.9 mV) was shifted 108 mV to the depolarization direction as compared with regular BK channels

formed by the intact BKα subunit ($V_{1/2}$ = 169.82 ± 0.05) (**Fig. 2D, Table 1**). Western blots results confirmed the expression of the concatenated BK channel construct (**Figure 2C**). To determine the contribution of each subunit to effect of the L312A mutation, four dimer mutants were constructed: $M1^{WT}M2^{L312A}$, $M1^{L312A}M2^{WT}$, $M3^{WT}M4^{L312A}$, and $M3^{L312A}M4^{WT}$ (**Figure 2D, Table 1**). The voltage dependence of channel activation was plotted for these mutants, and it was observed that the half mutations of L312A in the dimer mutants induced V1/2 shifts of approximately 47 ($M1^{L312A}M2^{WT}$), 57 ($M1^{WT}M2^{L312A}$), 51 ($M3^{L312A}M4^{WT}$), and 62 mV ($M3^{WT}M4^{L312A}$), respectively (**Figure 2D, Table 1**), which were approximately 50% of the V1/2 shift observed in the full L312A mutant ($V_{1/2}$ = 54.22 ± 1.7 mV). Furthermore, we observed that both dimer ($M1^{WT}M2^{L312A}$) and tetramer ($M1^{L312A}M2^{L312A}M3^{WT}M4^{WT}$) constructs, the half mutations caused V1/2 shifts of approximately 54 and 49 mV towards hyperpolarization compared to the wild-type BK channels (**Figure 2E, Table 1**). These results suggest that each subunit contributes equally to the effect of the L312A mutation in the BKα channel.

To test how the L312A mutant affects BK channel voltage gating, four kinds of mutations that gradually increased the mutant number in the tetramer constructs were constructed: $M1^{L312A}M2^{WT}M3^{WT}M4^{WT}$, $M1^{L312A}M2^{L312A}M3^{WT}M4^{WT}$, $M1^{L312A}M2^{L312A}M3^{L312A}M4^{WT}$, and $M1^{L312A}M2^{L312A}M3^{L312A}M4^{L312A}$ (**Figure 2F, Table 1**). By gradually increasing the number of mutant subunits in the tetramer constructs, the voltage dependence of the channel activation showed approximately 30 mV towards hyperpolarization for each subunit (**Figure 2G, Table 1**), suggesting that the effect of the L312A mutation is consistent, and mutation on each BKα subunit has an incremental effect on BK channel voltage gating. These findings reinforce the notion that each subunit within the BKα channel plays an equal role in determining the overall effect of the L312A mutation.

A single type of γ1 subunit complex produces a functionally all-or-none effect on the BK channel.

Recently, it was confirmed that a single γ1 subunit is sufficient to produce a gating shift similar to a set of four γ1 subunits, as demonstrated by functional reporter analysis in single-channel recordings [48-50]. Here, we aimed to investigate the molecular mechanisms underlying the atypical "all-or-none" modulatory function of γ subunits and the subunit stoichiometry of BK channel gating. To achieve this, we fused the C-terminal of the γ1 subunit to the N-terminal of the BKα S1 loop (**Figure 3A and 1C**). By co-transfecting the BKγ1-α fusion construct with the S0 and RCK2 domains, we observed similar V1/2 shifting in BKαγ1 (V1/2 = 20.84 ± 0.68 mV) and a deletion version of BKγ1-α (V1/2 = 33.09 ± 2.03 mV) (**Figure 3C, Table**

1). Next, we further generated functional concatenated tandem constructs containing 1 γ1 subunit with 2 or 4 copies of the BKα subunits (**Figure 3D**). The western blot assay revealed one major band for both the dimer (about 150 KD) and tetramer (about 270 KD) constructs (**Figure 3B**). Our results clearly demonstrated that both dimer and tetramer exhibited the atypical "all-or-none" modulatory. Specifically, the dimer BKγ1-αM1^{WT}M2^{WT} and tetramer BKγ1-αM1^{WT}M2^{WT}M3^{WT}M4^{WT} resulted in a reduction of 136 mV and 117 mV, respectively, in the shifts of BK channel $V_{1/2}$ induced by one γ1 ($V_{1/2}$ = 40.97 ± 1.29 mV) and two γ1 ($V_{1/2}$ = 61.42 ± 1.52 mV) subunits (**Figure 3D, Table 1**).

Screening of selectivity filter and deep-pore domain reveal three distinct types of subunit stoichiometry in BK channel modulation

Regarding the statement about γ1 subunit complex produces a functionally all-or-none effect on the BK channel, we hypothesize that there may be multiple modulation types in the BK channel. To explore the subunit stoichiometry and modulation types in BK channel, we constructed a series of mutations around the selectivity filter and deep-pore domain. In addition to L312A, we identified three other mutations (V288A, F303A and F307A) that can induce approximately 100 mV shifts in the V1/2 of BK channel toward the depolarization direction in the absent of Ca^{2+} (**Figure 4A and 4B**).

Firstly, we found that the V288A mutant, located at the selectivity filter, resulted in 93 mV reduction in the shifts of BK channel $V_{1/2}$ toward the depolarization direction in the presence of 10 μM Ca^{2+} (**Figure 4B and 4C**). To determine how this mutation regulates the selectivity filter, we constructed four mutations that gradually increased the mutant number in the tetramer constructs, similar to what we described for L312A earlier. These constructs were M1^{V288A}M2^{WT}M3^{WT}M4^{WT}, M1^{V288A}M2^{V288A}M3^{WT}M4^{WT}, M1^{V288A}M2^{V288A}M3^{V288A}M4^{WT}, and M1^{V288A}M2^{V288A}M3^{V288A}M4^{V288A} (**Figure 4C**). Unlike the additive regulation observed with L312A mutant in the deep pore, the V288A displayed an all-or-none effect. However, the all or none effect induced by V288A mutant is difference from that of the γ1 subunit. Our results shpwed that the half-activation voltages ($V_{1/2}$) of M1^{V288A}M2^{WT}M3^{WT}M4^{WT} (34.17 ± 1.37), M1^{V288A}M2^{V288A}M3^{WT}M4^{WT} (30.43 ± 2.08), and M1^{V288A}M2^{V288A}M3^{V288A}M4^{WT} (39.54 ± 1.69) were nearly the same as that of non-mutant BK channels (31.42 ± 2.39) in the presence of 10 μM Ca^{2+} (**Figure 4C**). However, only the full mutant construct (M1^{V288A}M2^{V288A}M3^{V288A}M4^{V288A}) resulted in a 93 mV reduction in the shifts of the BK channel $V_{1/2}$ toward depolarization in the presence of 10 μM Ca^{2+} (**Figure 4C**, Table 1). Our results demonstrated that the effect of V288A is only observed in the fully mutant BKα channel (**Figure 4C**, Table 1).

Previously, the Y294K mutant was shown to induce C-type inactivation in BK channels by an extreme low concentration of extracellular K^+ [51]. In this study, we performed single-channel analysis of the wide type and a series of mutations channels. We found that all recorded channels had the same reduced channel current. For example, the current for $M1^{Y294K}M2^{WT}M3^{WT}M4^{WT}$ was 26.6 pA compared to 31.6 pA for $M1^{WT}M2^{WT}M3^{WT}M4^{WT}$. Similarly, the currents for $M1^{Y294K}M2^{Y294K}M3^{WT}M4^{WT}$, $M1^{Y294K}M2^{Y294K}M3^{Y294K}M4^{WT}$, and $M1^{Y294K}M2^{Y294K}M3^{Y294K}M4^{Y294K}$ mutant channels were 21.6 pA, 16.5 pA and 11.6 pA, respectively, at 120 mV in the presence of 10 μM Ca^{2+} (**Figure 4D**). These results demonstrate that the Y294K mutant in the selectivity filter domain displays an incremental effect on the voltage gating of BK channel. Similar to the L312A and Y294K mutation, F303A, located in the deep-pore domain, also displayed an incremental effect on BK channel voltage gating (**Figure 4E**). We observed that the $V_{1/2}$ for the gradually increasing number of mutations in the BK tetramer, $M1^{L303A}M2^{WT}M3^{WT}M4^{WT}$, $M1^{L303A}M2^{L303A}M3^{WT}M4^{WT}$, and $M1^{L303A}M2^{L303A}M3^{L303A}M4^{L303A}$ were 46.86 ± 3.5 mV, 87.86 ± 5.03 mV, and 126.2 4± 3.5 mV, respectively. These values contributed approximately 40 mV toward the depolarization direction as compared to BK wide-type channels (**Figure 4F**).

Unlikely all the modulation types we mentioned above, we found that the mutant F307A in the deep-pore domain exhibited an “all-or-none” type of subunit stoichiometry in the modulation of BK channel (**Figure 4F**). Our results indicated that 1, 2, 4 mutants displayed a similar effect on BK channel voltage gating, resulting in reductions of 24.1 mV, 37.3 mV and 38.6 mV, respectively, in the shifts of BK channel $V_{1/2}$ towards the depolarization direction in the presence of 10 μM Ca^{2+} (**Figure 4F**).

Discussion

Concatenated tandem constructs have been extensively utilized in studying the subunit stoichiometry and mutation effects in other K+ channels, allowing for a deeper understanding of channel gating and regulation. However, the distinct architecture of BK channels has prevented the direct application of traditional concatenated tandem construct methodologies. The inability to physically connect the N- and C-termini of BK channel subunits in a concatenated manner has limited the exploration of subunit stoichiometry and modulation in BK channels. In this study, we employed a novel strategy and generated

functional concatenated tandem constructs by splicing BKα subunits into three protein constructs that could be co-expressed to form functional channels.

Previously, two types of modulation in BK channel gating have been demonstrated: incremental by β-subunit and all-or-none by γ1-subunit [27,52,53]. In our study, we aimed to investigate the presence of multiple modulation types in BK channels. To achieve this, we generated concatenated tandem constructs containing 2 or 4 copies of the BKα subunits by splicing BKα subunits into three protein constructs that could be co-expressed to form functional channels. We observed that the BK channels formed by concatenated tandem constructs are similar to intact channels in voltage and Ca^{2+} gating properties. Furthermore, to explore whether each subunit plays an equal role in modulation in BK channels, we employed a series of dimer and tetramer mutants of L312A were constructed. By performed inside-out patch clamp recording, our results demonstrated that the effect of the L312A mutation is consistent, and mutation on each BKα subunit has an incremental effect on BK channel voltage gating. These findings reinforce the notion that each subunit within the BKα channel plays an equal role in determining the overall effect of the L312A mutation. This suggests that our novel approach of splicing BKα into three protein constructs successfully resulted in the formation of functional BK channels, allowing us to investigate the subunit stoichiometry and modulation of BK channels in a concatenated tandem format.

Given that the pore-gate domain (PGD) control ion selectivity and K^+ permeation and played important role in BK channel voltage gating [54], we constructed a series of mutations around the selectivity filter and deep-pore domain. By further studying a series of concatenated tandem tetramer mutant constructs, interestingly, we observed that the BKγ subunits and mutations located at deep pore and selectivity filter displayed three distinct types of subunit stoichiometry in the modulation of BK channels.

In our study, we observed that a single BKγ1 subunit was sufficient to induce the full gating shift in BKα channels. This finding aligns with the results obtained by Gonzalez-Perez et al. [50], who utilized a Forster resonance energy transfer-based optical approach and a functional reporter in single-channel recordings. Although the precise mechanism underlying this effect was not fully elucidated in our study, we propose that there may be specific sites within the BKα channel, particularly in the pore-gate domain, where a single BKγ1 subunit can bind. This binding event could potentially induce a structural change that propagates through all four pore-forming subunits of the BK channel. As a result, the pore domain becomes more responsive to the activation of each of the four voltage sensors. Further investigations and studies will be necessary to validate this proposed mechanism and to gain a more comprehensive

understanding of how BKγ1 subunits modulate BKα channel gating. By elucidating the structural and functional implications of this interaction, we can advance our knowledge of BK channel regulation and pave the way for potential therapeutic interventions targeting these channels.

Similar to the L312A mutant, we observed that the Y294K and F303A mutations at the deep pore region of each BKα subunit had an incremental effect on BK channel voltage gating. This means that these mutations caused a gradual shift in the voltage dependence of channel activation. On the other hand, the V288A mutation at the selectivity filter exhibited an "all-or-none" effect. However, unlike the mutations in the deep pore region, the V288A mutation required mutations at all four BKα subunits to have a modulatory effect on channel gating. Mutations in only one, two, or three subunits had minimal impact on the gating behavior of the channel. Interestingly, the F307A mutation in the deep pore region displayed an atypical "all-or-none" modulatory function similar to that of the γ1 subunit. This mutation caused a complete shift in the channel's gating behavior, resembling the effect of the γ1 subunit on BK channel modulation. These findings highlight the complex nature of BK channel modulation and demonstrate the diverse effects that specific mutations can have on channel gating. Understanding these distinct modulatory mechanisms can provide insights into the functional roles of different regions and subunits in BK channel regulation. Importantly, using a concatenation strategy to study channel subunit stoichiometry is not without limitations. One potential issue is the unexpected assembly of subunits from different concatemers, which can lead to inconsistencies in the experimental results. Previous studies highlighted that in some cases, subunits from different concatemers can assemble together, leading to the formation of mixed channels with altered properties[55,56]. This unintended assembly can introduce variability and confound the interpretation of results. Indeed, some of our data does not perfectly align with initial expectations; for example, Figure 2G was not a straight line as expected. The complexity of protein assembly and the involvement of additional factors or interactions can contribute to variations in channel properties, including the formation of functional channels with small currents even in trimer constructs (data not shown). This indicated that obtaining convincing results for small shifts in channel properties can be challenging using this model. However, the results are conclusive for significant shifts caused by mutations, auxiliary subunits, and drugs.

In conclusion, our study employed a novel approach using concatenated tandem constructs to investigate the subunit stoichiometry and modulation of BK channels. By generating functional constructs with 2 or 4 copies of BKα subunits, we were able to uncover three distinct types of subunit stoichiometry in BK channel modulation. These included an additive effect, as well as two types of "all-or-none" effects on

BK channel voltage gating. The identified diversity in subunit stoichiometry provides valuable insights into the mechanisms underlying BK channel modulation by auxiliary γ subunits and mutations in the selectivity filter and deep-pore regions. This information not only enhances our understanding of BK channel function but also has implications for future studies on the modulation mechanisms of auxiliary subunits and drugs. The development of these novel concatenated tandem constructs for BK channels opens up new avenues for investigating the intricate regulatory mechanisms of BK channels and can contribute to the development of targeted interventions or therapies in the future. Overall, we have developed novel concatenated tandem constructs of BK channels and revealed three distinct types of subunit stoichiometry in BK channel modulation by auxiliary γ subunits and mutations at selectivity filter and deep-pore locations.

Table 1 Boltzmann-fit parameters of the voltage-dependent concatenated tandem BK channel activation in the wild-type, mutants in the absence and presence of intracellular Ca^{2+}.

Expression	Boltzmann fit parameters		
	$V_{1/2}$ (mV)	z	n[1]
BKα[2]	172 ± 3	1.16 ± 0.01	9
BKα(10 μM Ca^{2+})	22.54 ± 0.09	1.39 ±0.01	10
BKα$^{\Delta S0\Delta C}$ + BKα$^{\Delta 94\text{-}651}$-GFP	177.81 ± 1.51	1.18 ± 0.07	6
BKα$^{\Delta S0\Delta C}$ + BKα$^{\Delta 94\text{-}651}$-GFP (10 μM Ca^{2+})	22.17 ± 2.2	1.1 ±0.09	6
BKα (Dimer-M1M2) + BKα$^{\Delta 94\text{-}651}$-GFP	178.63 ± 1.03	1.13 ± 0.05	4
BKα (Dimer-M1M2) + BKα$^{\Delta 94\text{-}651}$-GFP (10 μM Ca^{2+})	22.62 ± 2.35	0.96 ± 0.07	5
BKα (Dimer-M3M4) + BKα$^{\Delta 94\text{-}651}$-GFP	180.1 ± 1.09	1.29 ±0.06	4
BKα (Dimer-M3M4) + BKα$^{\Delta 94\text{-}651}$-GFP (10 μM Ca^{2+})	22.19 ± 2.15	1.03 ± 0.08	5
BKα (Tetramer) + BKα$^{\Delta 94\text{-}651}$-GFP	177.82 ± 1.51	1.18 ± 0.07	6
BKα (Tetramer) + BKα$^{\Delta 94\text{-}651}$-GFP (10 μM Ca^{2+})	31.42 ± 2.39	0.93 ± 0.07	6
BKα (M1^{L312A}M2^{WT}) + BKα$^{\Delta 94\text{-}651}$-GFP	130.33± 1.58	0.95 ± 0.05	13
BKα (M1^{WT}M2^{L312A}) + BKα$^{\Delta 94\text{-}651}$-GFP	120.95± 2.11	0.85± 0.05	3
BKα (M3^{L312A}M4^{WT}) + BKα$^{\Delta 94\text{-}651}$-GFP	126 ± 1.25	0.85 ± 0.03	3
BKα (M3^{WT}M4^{L312A}) + BKα$^{\Delta 94\text{-}651}$-GFP	115.36± 1.77	0.84 ± 0.04	3
BKα(M1^{L312A}) + BKα$^{\Delta 94\text{-}651}$-GFP	61.9 ± 3.9	0.89 ± 0.02	6
BKα(M1^{L312A}M2^{WT}M3^{WT}M4^{WT}) + BKα$^{\Delta 94\text{-}651}$-GFP	150.17 ± 1.27	0.87 ± 0.01	7
BKα(M1^{L312A}M2^{L312A}M3^{WT}M4^{WT}) + BKα$^{\Delta 94\text{-}651}$-GFP	128.07±1.52	0.86±0.04	4
BKα(M1^{L312A}M2^{L312A}M3^{L312A}M4^{WT}) + BKα$^{\Delta 94\text{-}651}$-GFP	96.43± 1.08	0.80± 0.02	6
BKα(M1^{L312A}M2^{L312A}M3^{L312A}M4^{L312A}) + BKα$^{\Delta 94\text{-}651}$-GFP	54.22±1.7	1.07±0.07	6
BKα (V288A, 10 μM Ca^{2+})	115.42± 1.2	1.33 ± 0.07	3
BKα(M1^{V288A}M2^{WT}M3^{WT}M4^{WT}) + BKα$^{\Delta 94\text{-}651}$-GFP (10 μM Ca^{2+})	34.17±1.37	0.89±0.04	4

BKα(M1^{V288A}M2^{V288A}M3^{WT}M4^{WT}) + BKα$^{\Delta 94-651}$-GFP (10 μM Ca^{2+})	30.43± 2.08	0.96± 0.07	3
BKα(M1^{V288A}M2^{V288A}M3^{WT}M4^{V288A}) + BKα$^{\Delta 94-651}$-GFP (10 μM Ca^{2+})	39.54± 1.69	0.94± 0.05	3
BKα (M1^{V288A}M2^{V288A}M3^{V288A} M4^{V288A}) + BKα$^{\Delta 94-651}$-GFP (10 μM Ca^{2+})	117.12±1.01	1.11±0.05	4
BKα(M1^{F303A}M2^{WT}M3^{WT}M4^{WT}) + BKα$^{\Delta 94-651}$-GFP (10 μM Ca^{2+})	46.86±3.5	1.03±0.11	4
BKα(M1^{F303A}M2^{F303A}M3^{WT}M4^{WT}) + BKα$^{\Delta 94-651}$-GFP (10 μM Ca^{2+})	87.86± 5.03	0.96± 0.1	3
BKα(M1^{F303A}M2^{F303A}M3^{F303A}M4^{F303A}) + BKα$^{\Delta 94-651}$-GFP (10 μM Ca^{2+})	126.24± 3.5	0.73± 0.05	3
BKα(M1^{V307A}M2^{WT}M3^{WT}M4^{WT}) + BKα$^{\Delta 94-651}$-GFP (10 μM Ca^{2+})	55.5±1.4	0.93±0.11	4
BKα(M1^{V307A}M2^{V307A}M3^{WT}M4^{WT}) + BKα$^{\Delta 94-651}$-GFP (10 μM Ca^{2+})	68.7± 3	0.72± 0.04	6
BKα(M1^{V307A}M2^{V307A}M3^{V307A}M4^{V307A}) + BKα$^{\Delta 94-651}$-GFP (10 μM Ca^{2+})	70± 1.3	0.98± 0.05	5
BKα-γ1	20.84 ± 0.68	1.05 ± 0.03	4
BKγ1-α-M1$^{\Delta S0 \Delta C}$ + BKα$^{\Delta 94-651}$-GFP	33.09 ± 2.03	0.92 ± 0.06	4
BKγ1-α(Dimer) + BKα$^{\Delta 94-651}$-GFP	61.42 ± 1.52	0.83 ± 0.03	5
BKγ1-α(Tetramer) + BKα$^{\Delta 94-651}$-GFP	40.97 ± 1.29	0.95 ± 0.04	6

[1] The number of recorded excised inside-out patches from different HEK293 cells.

[2] Unless indicated with a specific Ca^{2+} concentration, all recording were done in the virtual absence of intracellular free Ca^{2+}.

Figure legend

Figure 1. Novel concatenated tandem constructs of BK channel. (A) Representative traces of recorded BK channel currents in response to the depolarization of the membrane potential from −80 mV in 20-mV steps for selected expression constructs. **(B)** Western blot of transfected with each concatemeric channel constructs from HEK293 cells, as indicated (Dimer = BKα (Dimer-M3M4), Tetramer = BKα (M1M2M3M4)). **(C-E)** Voltage dependence of BK channel activation for channels formed by the BKα Monomer (C), Dimer (D) and Tetramer (E) in the virtual absence of Ca^{2+} and in the presence of 10 μM Ca^{2+} (n = 4-10). Error bars represent +/- SEM.

Figure 2. The deep pore L312A mutation on each BKα subunit shows an incremental effect on BK channel voltage gating. (A) Top view of the structure of human BK channel, hSlo1 (6V3G), highlighting transmembrane domain (cyan) and L312 site (purple) in the absent of Ca^{2+}. **(B)** Side view of the structure of human BK channel, hSlo1 (6V3G). For clarity, RCK domains and domains in the front and back have been removed. L312 site is shown as purple ball. **(C)** Western blots obtained from HEK293 cells expressing different of L312A mutant in the tetrameric constructs of BKα proteins. **(D)** Voltage dependence of BK channel activation for channels formed by different subunit mutant of L312A in BKα (Dimer) channels constructs. **(E)** Voltage dependence of L312A mutant BK channel activation for channels formed by BKα (Dimer) and BKα (Tetramer) channels constructs. **(F-G)** Voltage dependence of BK channel activation for channels formed by different subunit mutant of L312A in BKα (Tetramer) channels constructs. Error bars represent +/- SEM.

Figure 3. Novel concatenated tandem constructs of BKγ1-α reveal one BKγ1 subunit suffices to produce an "all-or-none" effect. (A) Representative traces of recorded BK channel currents in response to the depolarization of the membrane potential from −80 mV in 20-mV steps for selected expression constructs. **(B)** Western blots obtained from HEK293 cells expressing different BKγ1-α in the dimeric and tetrameric constructs of BKα proteins constructs. **(C-D)** Voltage dependence of BK channel activation for channels formed by the BKγ1-α Monomer, Dimer and Tetramer (n = 4-10). Error bars represent +/- SEM.

Figure 4. Screening of selectivity filter and deep-pore domain reveal three distinct types of subunit stoichiometry in BK channel modulation. (A) Mutant scan of selectivity filter and deep pore domains. **(B)** Side view of the structure of human BK channel, hSlo1 (6V3G). For clarity, RCK domains and

domains in the front and back have been removed. V288A, Y294K, F303A and F307A sites are shown as purple ball. **(C)** Voltage dependence of BK channel activation for channels formed by different subunit mutant of V288A in BKα (Tetramer) channels constructs. (**D)** A current record from a membrane patch with a single BK channel for 10 μM intracellular Ca^{2+} and +120 mV. Channel opening is indicated by upward current steps and channel closing by downward current steps. (**E)** Voltage dependence of BK channel activation for channels formed by different subunit mutant of F303A in BKα (Tetramer) channels constructs. (**F)** Voltage dependence of BK channel activation for channels formed by different subunit mutant of F307A in BKα (Tetramer) channels constructs. Error bars represent +/- SEM.

Figure 1

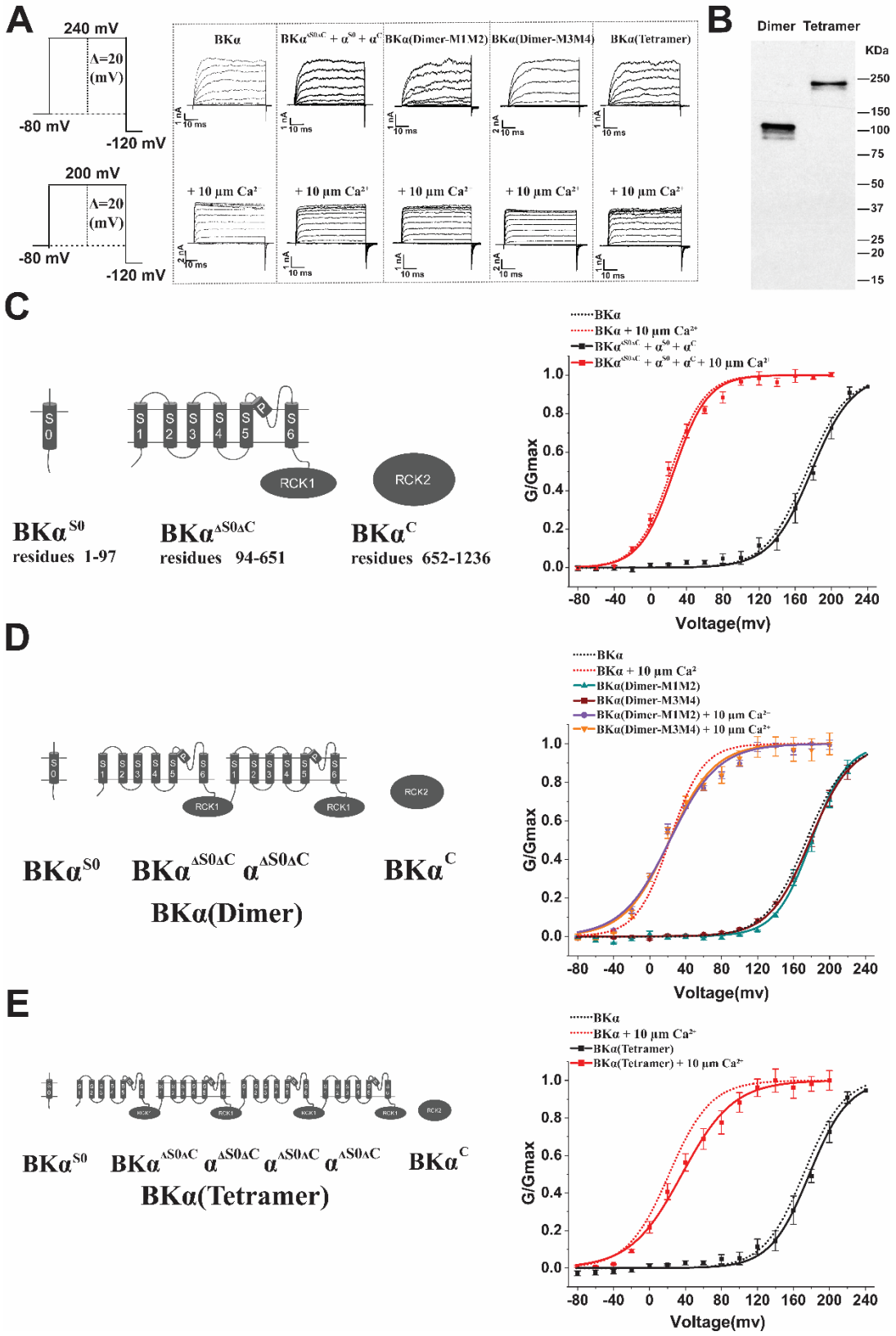
A
240 mV
Δ=20 (mV)
-80 mV
-120 mV
200 mV
BKα
BKα^ΔS0ΔC + α^S0 + α^C
BKα(Dimer-M1M2)
BKα(Dimer-M3M4)
BKα(Tetramer)
+ 10 μm Ca²⁺
B
Dimer Tetramer
KDa
250
150
100
75
50
37
25
20
15
C
BKα^S0
residues 1-97
BKα^ΔS0ΔC
residues 94-651
BKα^C
residues 652-1236
RCK1
RCK2
BKα
BKα + 10 μm Ca²⁺
BKα^ΔS0ΔC + α^S0 + α^C
BKα^ΔS0ΔC + α^S0 + α^C + 10 μm Ca²⁺
G/Gmax
Voltage(mv)
D
BKα^S0
BKα^ΔS0ΔC α^ΔS0ΔC
BKα(Dimer)
BKα^C
BKα(Dimer-M1M2)
BKα(Dimer-M3M4)
BKα(Dimer-M1M2) + 10 μm Ca²⁺
BKα(Dimer-M3M4) + 10 μm Ca²⁺
E
BKα^S0
BKα^ΔS0ΔC α^ΔS0ΔC α^ΔS0ΔC α^ΔS0ΔC
BKα(Tetramer)
BKα^C
BKα(Tetramer)
BKα(Tetramer) + 10 μm Ca²⁺

Figure 2

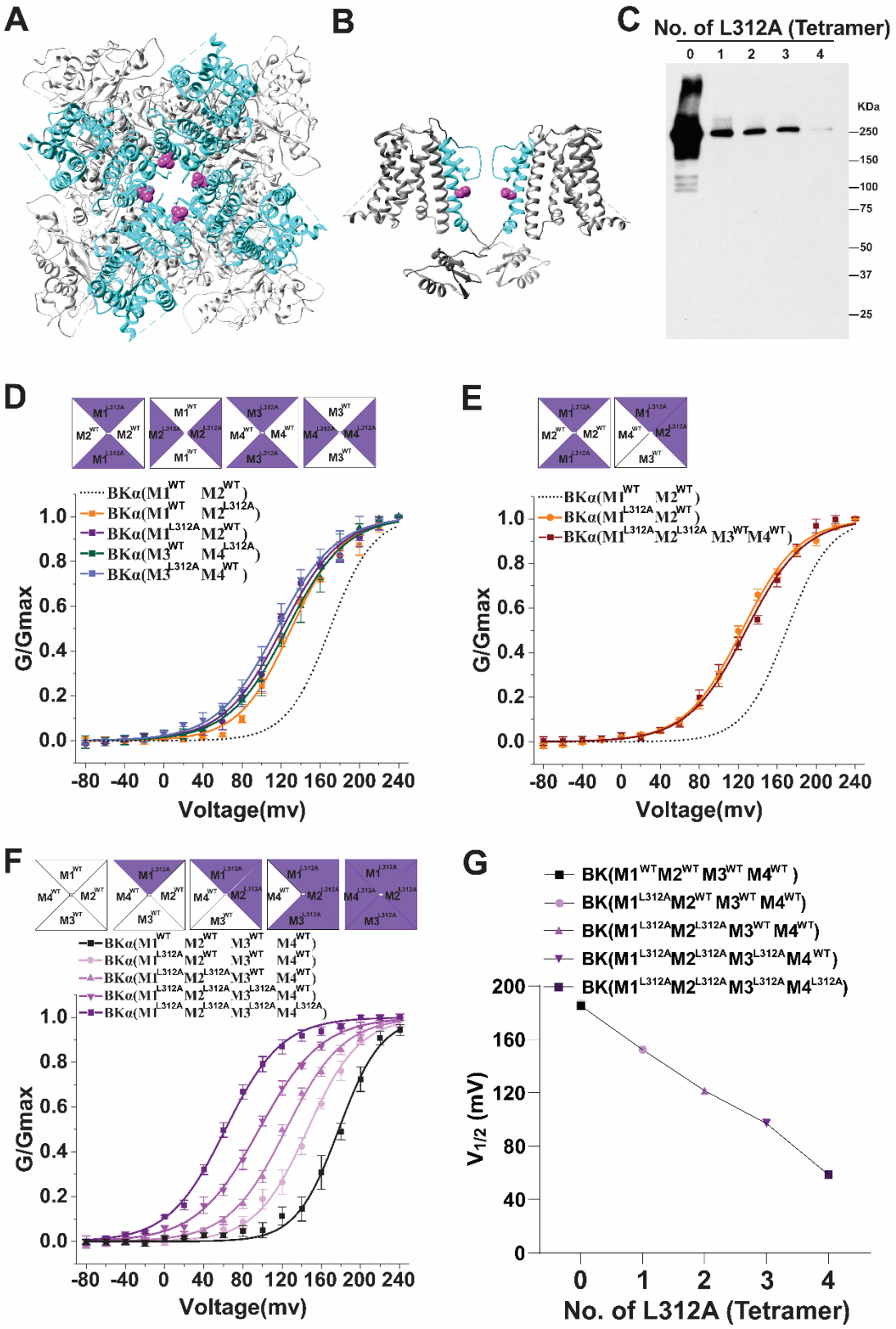
A
B
C
No. of L312A (Tetramer)
0 1 2 3 4
KDa
250
150
100
75
50
37
25
D
E
F
G
G/Gmax
Voltage(mv)
BKα(M1WT M2WT)
BKα(M1WT M2L312A)
BKα(M1L312A M2WT)
BKα(M3WT M4L312A)
BKα(M3L312A M4WT)
BKα(M1L312A M2L312A M3WT M4WT)
BK(M1WT M2WT M3WT M4WT)
BK(M1L312A M2WT M3WT M4WT)
BK(M1L312A M2L312A M3WT M4WT)
BK(M1L312A M2L312A M3L312A M4WT)
BK(M1L312A M2L312A M3L312A M4L312A)
V1/2 (mV)
No. of L312A (Tetramer)

Figure 3

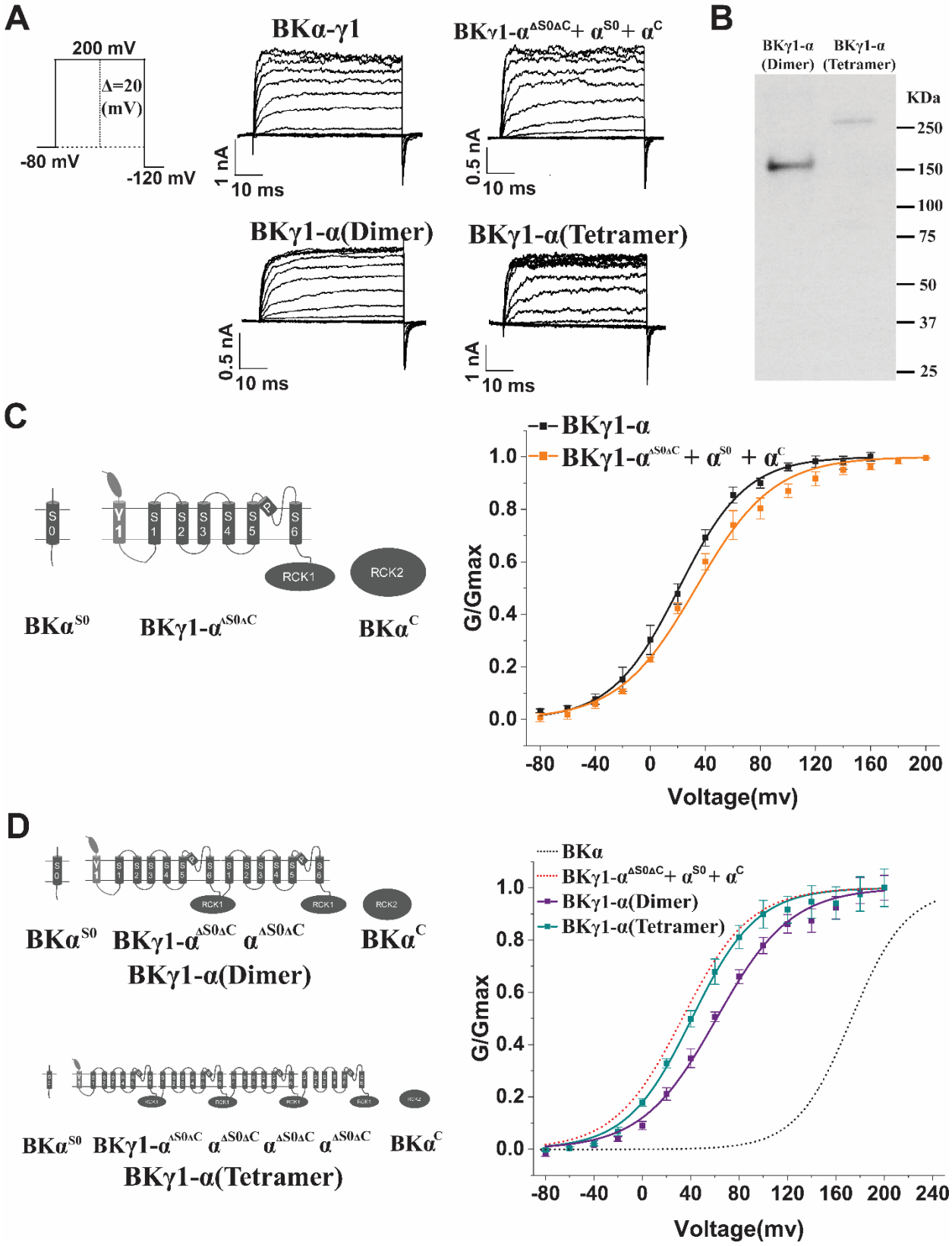
A
200 mV
Δ=20 (mV)
-80 mV
-120 mV
BKα-γ1
BKγ1-α^ΔS0ΔC+ α^S0+ α^C
1 nA
10 ms
0.5 nA
10 ms
BKγ1-α(Dimer)
BKγ1-α(Tetramer)
0.5 nA
10 ms
1 nA
10 ms
B
BKγ1-α (Dimer)
BKγ1-α (Tetramer)
KDa
250
150
100
75
50
37
25
C
S0
Y1
S1
S2
S3
S4
S5
S6
RCK1
RCK2
BKα^S0
BKγ1-α^ΔS0ΔC
BKα^C
BKγ1-α
BKγ1-α^ΔS0ΔC + α^S0 + α^C
G/Gmax
Voltage(mv)
D
BKα^S0 BKγ1-α^ΔS0ΔC α^ΔS0ΔC BKα^C
BKγ1-α(Dimer)
BKα^S0 BKγ1-α^ΔS0ΔC α^ΔS0ΔC α^ΔS0ΔC α^ΔS0ΔC BKα^C
BKγ1-α(Tetramer)
BKα
BKγ1-α^ΔS0ΔC+ α^S0+ α^C
BKγ1-α(Dimer)
BKγ1-α(Tetramer)
G/Gmax
Voltage(mv)

Figure 4

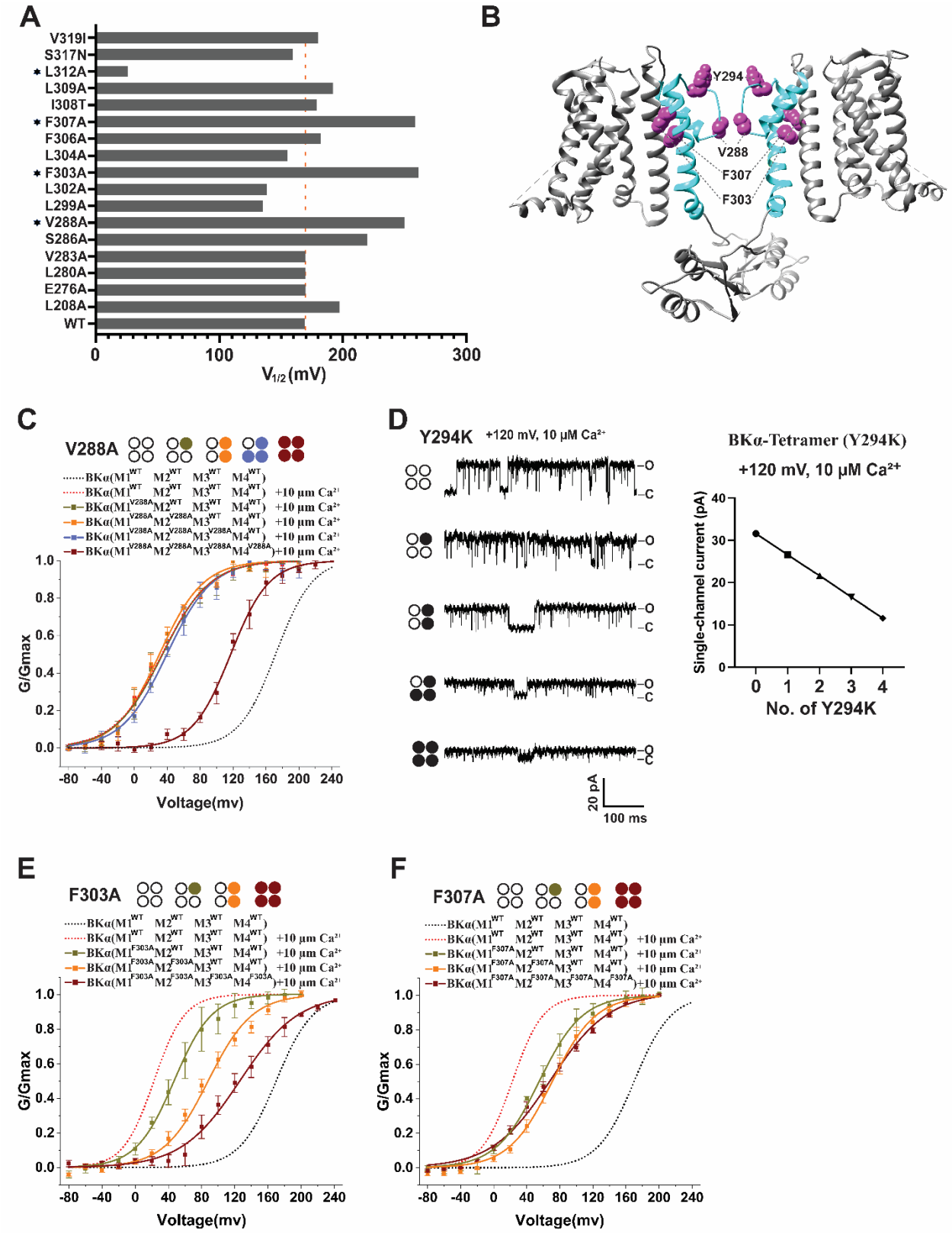
A
V319I
S317N
* L312A
L309A
I308T
* F307A
F306A
L304A
* F303A
L302A
L299A
* V288A
S286A
V283A
L280A
E276A
L208A
WT
0
100
200
300
V1/2 (mV)
B
Y294
V288
F307
F303
C
V288A
G/Gmax
Voltage(mv)
D
Y294K +120 mV, 10 μM Ca2+
O
C
20 pA
100 ms
BKα-Tetramer (Y294K)
+120 mV, 10 μM Ca2+
Single-channel current (pA)
No. of Y294K
E
F303A
G/Gmax
Voltage(mv)
F
F307A
G/Gmax
Voltage(mv)

Reference

1 Ghatta, S., Nimmagadda, D., Xu, X. & O'Rourke, S. T. Large-conductance, calcium-activated potassium channels: structural and functional implications. *Pharmacol Ther* **110**, 103-116 (2006).

2 Salkoff, L., Butler, A., Ferreira, G., Santi, C. & Wei, A. High-conductance potassium channels of the SLO family. *Nat. Rev. Neurosci.* **7**, 921-931 (2006).

3 Wu, Y., Yang, Y., Ye, S. & Jiang, Y. Structure of the gating ring from the human large-conductance Ca(2+)-gated K(+) channel. *Nature* **466**, 393-397, doi:10.1038/nature09252 (2010).

4 Yuan, P., Leonetti, M. D., Hsiung, Y. & MacKinnon, R. Open structure of the Ca2+ gating ring in the high-conductance Ca2+-activated K+ channel. *Nature* **481**, 94-97, doi:10.1038/nature10670 (2011).

5 Hite, R. K., Tao, X. & MacKinnon, R. Structural basis for gating the high-conductance Ca2+-activated K+ channel. *Nature* **541**, 52-57, doi:10.1038/nature20775 (2017).

6 Tao, X., Hite, R. K. & MacKinnon, R. Cryo-EM structure of the open high-conductance Ca2+-activated K+ channel. *Nature* **541**, 46-51, doi:10.1038/nature20608 (2017).

7 Tao, X. & MacKinnon, R. Molecular structures of the human Slo1 K(+) channel in complex with beta4. *eLife* **8**, doi:10.7554/eLife.51409 (2019).

8 Raisch, T. *et al.* Small molecule modulation of the Drosophila Slo channel elucidated by cryo-EM. *Nature communications* **12**, 7164, doi:10.1038/s41467-021-27435-w (2021).

9 Yang, H., Zhang, G. & Cui, J. BK channels: multiple sensors, one activation gate. *Frontiers in physiology* **6**, 29, doi:10.3389/fphys.2015.00029 (2015).

10 Wu, Y., Yang, Y., Ye, S. & Jiang, Y. Structure of the gating ring from the human large-conductance Ca(2+)-gated K(+) channel. *Nature* **466**, 393-397 (2010).

11 Yuan, P., Leonetti, M. D., Pico, A. R., Hsiung, Y. & MacKinnon, R. Structure of the human BK channel Ca2+-activation apparatus at 3.0 A resolution. *Science* **329**, 182-186, doi:10.1126/science.1190414 (2010).

12 Shi, J. *et al.* Mechanism of magnesium activation of calcium-activated potassium channels. *Nature* **418**, 876-880, doi:10.1038/nature00941 (2002).

13 Xia, X. M., Zeng, X. & Lingle, C. J. Multiple regulatory sites in large-conductance calcium-activated potassium channels. *Nature* **418**, 880-884, doi:10.1038/nature00956 (2002).

14 Yusifov, T., Savalli, N., Gandhi, C. S., Ottolia, M. & Olcese, R. The RCK2 domain of the human BKCa channel is a calcium sensor. *Proceedings of the National Academy of Sciences of the United States of America* **105**, 376-381, doi:10.1073/pnas.0705261105 (2008).

15 Guan, X., Li, Q. & Yan, J. Relationship between auxiliary gamma subunits and mallotoxin on BK channel modulation. *Scientific reports* **7**, 42240, doi:10.1038/srep42240 (2017).

16 Li, Q. & Yan, J. Modulation of BK Channel Function by Auxiliary Beta and Gamma Subunits. *International review of neurobiology* **128**, 51-90, doi:10.1016/bs.irn.2016.03.015 (2016).

17 Gonzalez-Perez, V. & Lingle, C. J. Regulation of BK Channels by Beta and Gamma Subunits. *Annual review of physiology* **81**, 113-137, doi:10.1146/annurev-physiol-022516-034038 (2019).

18 Dudem, S. *et al.* LINGO1 is a regulatory subunit of large conductance, Ca(2+)-activated potassium channels. *Proceedings of the National Academy of Sciences of the United States of America* **117**, 2194-2200, doi:10.1073/pnas.1916715117 (2020).

19 Sun, X., Zaydman, M. A. & Cui, J. Regulation of Voltage-Activated K(+) Channel Gating by Transmembrane beta Subunits. *Frontiers in pharmacology* **3**, 63, doi:10.3389/fphar.2012.00063 (2012).

20 Contreras, G. F., Neely, A., Alvarez, O., Gonzalez, C. & Latorre, R. Modulation of BK channel voltage gating by different auxiliary beta subunits. *Proc. Natl. Acad. Sci. U.S.A.* **109**, 18991-18996, doi:10.1073/pnas.1216953109 (2012).

21 Zhang, J. & Yan, J. Regulation of BK channels by auxiliary gamma subunits. *Frontiers in physiology* **5**, 401, doi:10.3389/fphys.2014.00401 (2014).

22 Cox, D. H. & Aldrich, R. W. Role of the beta1 subunit in large-conductance Ca(2+)-activated K(+) channel gating energetics. Mechanisms of enhanced Ca(2+) sensitivity. *J Gen Physiol* **116**, 411-432 (2000).

23 Behrens, R. *et al.* hKCNMB3 and hKCNMB4, cloning and characterization of two members of the large-conductance calcium-activated potassium channel beta subunit family. *FEBS Lett.* **474**, 99-106 (2000).

24 Brenner, R., Jegla, T. J., Wickenden, A., Liu, Y. & Aldrich, R. W. Cloning and functional characterization of novel large conductance calcium-activated potassium channel beta subunits, hKCNMB3 and hKCNMB4. *J. Biol. Chem.* **275**, 6453-6461 (2000).

25 Solaro, C. R. & Lingle, C. J. Trypsin-sensitive, rapid inactivation of a calcium-activated potassium channel. *Science* **257**, 1694-1698 (1992).

26 Yan, J. & Aldrich, R. W. LRRC26 auxiliary protein allows BK channel activation at resting voltage without calcium. *Nature* **466**, 513-516, doi:10.1038/nature09162 (2010).

27 Yan, J. & Aldrich, R. W. BK potassium channel modulation by leucine-rich repeat-containing proteins. *Proceedings of the National Academy of Sciences of the United States of America* **109**, 7917-7922, doi:10.1073/pnas.1205435109 (2012).

28 Chen, G., Li, Q., Webb, T. I., Hollywood, M. A. & Yan, J. BK channel modulation by positively charged peptides and auxiliary gamma subunits mediated by the Ca2+-bowl site. *J Gen Physiol* **155**, doi:10.1085/jgp.202213237 (2023).

29 Chen, G. L., Q.; Yan, J. The leucine-rich repeat domains of BK channel auxiliary γ subunits regulate their expression, trafficking, and channelmodulation functions. *J. Biol. Chem.* **298**, 101664 (2022).

30 Li, Q., Guan, X., Yen, K., Zhang, J. & Yan, J. The single transmembrane segment determines the modulatory function of the BK channel auxiliary gamma subunit. *J Gen Physiol* **147**, 337-351, doi:10.1085/jgp.201511551 (2016).

31 Li, Q., Fan, F., Kwak, H.R., and Yan, J. . Molecular basis for differential modulation of BK channel voltage-dependent gating by gamma auxiliary subunits. . *J. Gen. Physiol* **145**, 543–554 (2015).

32 Gonzalez-Perez, V., Xia, X.M., and Lingle C.J. . Functional regulation of BK potassium channels by γ1 auxiliary subunits. *Proc Natl Acad Sci USA* **111**, 4868–4873 (2014).

33 Wang, Y. W., Ding, J. P., Xia, X. M. & Lingle, C. J. Consequences of the stoichiometry of Slo1 alpha and auxiliary beta subunits on functional properties of large-conductance Ca2+-activated K+ channels. *J. Neurosci.* **22**, 1550-1561 (2002).

34 Murray, C. I. *et al.* Unnatural amino acid photo-crosslinking of the IKs channel complex demonstrates a KCNE1:KCNQ1 stoichiometry of up to 4:4. *eLife* **5**, doi:10.7554/eLife.11815 (2016).

35 Nakajo, K., Ulbrich, M. H., Kubo, Y. & Isacoff, E. Y. Stoichiometry of the KCNQ1 - KCNE1 ion channel complex. *Proceedings of the National Academy of Sciences of the United States of America* **107**, 18862-18867, doi:10.1073/pnas.1010354107 (2010).

36 Kitazawa, M., Kubo, Y. & Nakajo, K. The stoichiometry and biophysical properties of the Kv4 potassium channel complex with K+ channel-interacting protein (KChIP) subunits are variable, depending on the relative expression level. *The Journal of biological chemistry* **289**, 17597-17609, doi:10.1074/jbc.M114.563452 (2014).

37 Gonzalez-Perez, V., Xia, X. M. & Lingle, C. J. Functional regulation of BK potassium channels by gamma1 auxiliary subunits. *Proc. Natl. Acad. Sci. U.S.A.* **111**, 4868-4873, doi:10.1073/pnas.1322123111 (2014).

38 Hurst, R. S., North, R. A. & Adelman, J. P. Potassium channel assembly from concatenated subunits: effects of proline substitutions in S4 segments. *Receptors & channels* **3**, 263-272 (1995).

39 Hurst, R. S., Kavanaugh, M. P., Yakel, J., Adelman, J. P. & North, R. A. Cooperative interactions among subunits of a voltage-dependent potassium channel. Evidence from expression of concatenated cDNAs. *The Journal of biological chemistry* **267**, 23742-23745 (1992).

40 Fahlke, C., Rhodes, T. H., Desai, R. R. & George, A. L., Jr. Pore stoichiometry of a voltage-gated chloride channel. *Nature* **394**, 687-690, doi:10.1038/29319 (1998).

41 Minier, F. & Sigel, E. Techniques: Use of concatenated subunits for the study of ligand-gated ion channels. *Trends in pharmacological sciences* **25**, 499-503, doi:10.1016/j.tips.2004.07.005 (2004).

42 White, M. M. Pretty subunits all in a row: using concatenated subunit constructs to force the expression of receptors with defined subunit stoichiometry and spatial arrangement. *Molecular pharmacology* **69**, 407-410, doi:10.1124/mol.105.020727 (2006).

43 Sack, J. T., Shamotienko, O. & Dolly, J. O. How to validate a heteromeric ion channel drug target: assessing proper expression of concatenated subunits. *J Gen Physiol* **131**, 415-420, doi:10.1085/jgp.200709939 (2008).

44 Li, Q., Guan, X., Yen, K., Zhang, J., and Yan, J. The single transmembrane segment determines the modulatory function of the BK channel auxiliary gamma subunit. *J. Gen. Physiol.* **147** (2016).

45 Guanxing Chen, Q. L., Timothy I. Webb, Mark A. Hollywood, and Jiusheng Yan. BK channel modulation by positively charged peptides and auxiliary ã subunits mediated by the Ca2+-bowl site. *J. Gen. Physiol.* **155**, e202213237 (2023).

46 Chen X, Y. Y., and Aldrich RW. BK channel opening involves side-chain reorientation of multiple deep-pore residues. *Proc. Natl. Acad. Sci. USA* **111**, E79–E88 (2013).

47 Wu Y, X. Y., Wang S, Yi H, Li H, Pan N, Horrigan FT, Wu Y , and Ding J. Intersubunit Coupling in the Pore of BK Channels. *Journal of Biological Chemistry* **284**, 23353–23363 (2009).

48 Gonzalez-Perez V, X. X., Lingle CJ. Functional regulation of BK potassium channels by ã1 auxiliary subunits. *Proc Natl Acad Sci USA* **111**, 4868–4873 (2014).

49 Gonzalez-Perez, V., and C.J. Lingle. Regulation of BK Channels by Beta and Gamma Subunits. . *Annu Rev Physiol.* **81**, 113-137 (2019).

50 Gonzalez-Perez V , J. M., Xia XM, and Lingle CJ. Regulatory γ1 subunits defy symmetry in functional modulation of BK channels. *Proc Natl Acad Sci USA* **115**, 9923-9928 (2018).

51 Jiusheng Yan, Q. L., and Richard W. Aldrich. Closed state-coupled C-type inactivation in BK channels. *Proc Natl Acad Sci USA* **113**, 6991–6996 (2016).

52 Wang YW, D. J., Xia XM, Lingle CJ. Consequences of the stoichiometry of Slo1 α and auxiliary β subunits on functional properties of large-conductance Ca2+-activated K+ channels. *J Neurosci* **22**, 1550-1561 (2002).

53 Yan, J., and Aldrich, R.W. LRRC26 auxiliary protein allows BK channel activation at resting voltage without calcium. *Nature* **466**, 513-516 (2010).

54 Doyle DA, M. J., Pfuetzner RA, Kuo A, Gulbis JM, Cohen SL, et al. The structure of the potassium channel: molecularbasisof K+ conduction and selectivity. *Science* **280**, 68-77 (1998).

55 Ken McCormack, L. L., Linda E. Iverson, Mark A. Tanouye, and Fred J. Sigworth. Tandem linkage of Shaker K+ channel subunits does not ensure the stoichiometry of expressed channels. *Biophys. J.* **63**, 1406–1411 (1992).

56 Jon T. Sack, O. S., and J. Oliver Dolly. How to Validate a Heteromeric Ion Channel Drug Target: Assessing Proper Expression of Concatenated Subunits. *J. Gen. Physiol.* **131**, 415–420 (2008).